Available online at www.sciencedirect.com
ScienceDirect
Journal of Power Sources 164 (2007) 154–165
JOURNAL OF POWER SOURCES
www.elsevier.com/locate/jpowsour

Electroosmotic effect on flows in a serpentine microchannel with varying zeta potential

Auro Ashish Saha [a], Sushanta K. Mitra [a,*], Xianguo Li [b]

[a] *Department of Mechanical Engineering, Indian Institute of Technology Bombay, Mumbai 400076, India*
[b] *Department of Mechanical Engineering, University of Waterloo, Waterloo, Ont. N2L 3G1, Canada*

Received 2 August 2006; received in revised form 25 August 2006; accepted 15 September 2006
Available online 20 November 2006

Abstract

Electroosmosis is widely observed in different micro-scale flows. Flow modification due to electroosmosis is important for applications related to fuel cells such as micro direct methanol fuel cells and micro-scale devices. Mechanism for delivering methanol into the micro-fuel cell is very important process affecting its power density and often they need to be stand alone systems with no external pumps or other ancillary devices to eliminate the parasitic power loss accounting from fuel feed. In this study, numerical simulation has been carried out for the electroosmotic effect on pressure-driven flows in a serpentine microchannel whose side walls are subjected to variable zeta potentials. It is observed that for a non-uniform zeta potential, the secondary vortex pair and their strength of motion generated by electroosmosis is modified asymmetrically, corresponding to the degree of the variation in and the magnitude of the zeta potential. It is also found that the flow profiles are quite different for variable zeta potentials as compared to a constant zeta potential applied on the channel walls. The flow phenomena at the bend of the serpentine channel has also been investigated, and flow control is possible by regulating the applied zeta potential on the channel walls. It is observed that vortices shift in a clockwise direction as the applied zeta potential is increased on the walls of the serpentine channel. Formation of additional vortices has also been observed for very low values of applied zeta potential.

Keywords: Serpentine microchannel; Electroosmotic flow; Numerical; Three-dimensional; Zeta potential

1. Introduction

The convective transport in micro domain is of great importance as it applies to various application such as Micro Electro Mechanical Systems (MEMS) devices, micro-heat exchangers, micro-fuel cells, etc. [1]. Electroosmosis is the bulk movement of liquid near a stationary surface due to an externally applied electric field [2]. In fuel cells, the typical fuel such as hydrogen for Proton Exchange Membrane (PEM) or methanol for Direct Methanol Fuel Cell (DMFC), flows through the serpentine flow field present in the bi-polar plates of the cell. Due to the electric potential generated in the micro-fuel cell, a potential gradient is developed in the bi-polar plate, the direction of which is perpendicular to the flow direction. The presence of an aqueous solution in the flow field such as methanol in case of DMFC, results in electroosmosis driven flow, which is of interest for micro-fuel cell applications.

There have been a few studies reported in the field of electroosmosis driven flow in micro DMFC. Karimi and Li [3] have modeled the electroosmotic flow in the fuel cell membrane including the electrokinetic effect. They have modeled the membrane pore to determine the electroosmotic flow through the membrane for different geometrical and operating conditions. They have reported a nonlinear increase in electroosmotic flow with increase in pore size and found that the electroosmotic drag coefficient increases linearly with pore size.

Several researchers have investigated the effect of varying zeta potential on electroosmotic flow (EOF) in microchannels [4–8]. Such EOF are in the direction of the pressure driven flow. The characteristics of EOF in a microchannel depend upon the nature of the zeta potential, i.e., whether it is uniform or nonuniform. Fu et al. [4] used Nernst–Planck equation along with a Navier–Stokes solution to model the EOF that occurs when a step change in zeta potential is applied. The results indicate that a step change in zeta potential causes a significant

* Corresponding author. Tel.: +91 22 2576 7513; fax: +91 22 2572 6875.
E-mail addresses: skmitra@me.iitb.ac.in (S.K. Mitra), x6li@uwaterloo.ca (X. Li).

0378-7753/$ – see front matter © 2006 Elsevier B.V. All rights reserved.
doi:10.1016/j.jpowsour.2006.09.106

Nomenclature

C_0	ionic concentration in bulk solution
D_h	hydraulic diameter of channel cross section
E	electric field intensity
F	Faraday's constant
H_c	channel depth
L	half length of section of straight segment of channel
R_c	radius of curvature of channel axis at U-bend
Re	Reynolds number
R_u	universal gas constant
u	velocity component in x-direction
v	velocity component in y-direction
V_{inlet}	velocity of fluid at inlet
w	velocity component in z-direction
W_c	channel width
z_e	valence number of univalent fluid
$z_{+/-}$	valence number of the positive/negative ions in the fluid

Greek letters

ϵ	permittivity of fluid
λ	Debye length
μ	viscosity of fluid
ϕ	applied potential
ψ	potential due to electrical double layer
ρ	density of fluid
ρ_E	charge density
ζ_w	zeta potential or wall potential

variation in the velocity profile and also in the pressure distribution.

Micro-scale debris and manufacturing irregularities during fabrication of microchannels, and adsorption of organics during analysis of microchannels produce nonuniform zeta potential distributions along the channel walls. Herr et al. [5] have shown the influence of zeta potential on the velocity profile and sample dispersion rate for electroosmotic flow in cylindrical capillaries with nonuniform zeta potential distribution. Similarly, Chen et al. [6] investigated numerically the effects of step change in zeta potential in a cylindrical microchannel on electroosmotic flow. It is observed that the variable zeta potential along the flow direction generated regions of positive and negative pressure gradients in the flow field. Lee et al. [7] studied electroosmotic flow in a cylindrical microchannel with non-uniform zeta potential distribution. They showed formation of distorted electroosmotic velocity profiles and flow circulation resulting from the axial variation of the zeta potential. However, these studies are related to straight microchannels only.

Zhang et al. [8] studied the two-dimensional flow pattern in microchannels with large aspect ratios with heterogeneous zeta potentials, and discuss the formation of secondary EOF's generated by wavelike zeta potential. Their results show that the heterogeneous zeta potentials could generate complex flow patterns and enhance mixing. However, their study may not be representative for microchannels with nearly square cross section.

Souders et al. [9] have studied combined electroosmotic and pressure driven flows in a three-dimensional microchannel with walls covered by charged bands. Under the influence of electroosmotic flow only, it is found that there is a significant amount of fluid folding and stretching. By adding pressure gradient against electroosmotic flow, they showed an increase in the fluid particle residence time. The helical flow structure is also observed for this combined electroosmotic and pressure driven flow.

Fuel feed into the micro-fuel cell is an important process affecting its power density and often there is a need to minimize power loss accounting from fuel delivery. Buie et al. [10] presented a novel design and performance of a planar silicon electroosmotic pump (EO) for methanol fuel delivery in DMFC. Though the EO pump could not deliver enough pressure head for fuel delivery, nevertheless it was interesting to note that the micro DMFC has shown to have improved polarization and power density characteristics with the EO pump. The study in particular emphasizes the performance enhancement due the combined mechanism of electroosmotic phenomena and diffusion for fuel delivery.

More recently, Rawool and Mitra [12] studied the transport of methanol in micro-fuel cell under the applied potential which is perpendicular to the direction of the flow. Such conditions are unique to fuel cell applications, and are not studied prior to this work. However, in their work, the side walls are subjected to a constant zeta potential, which is not always the case in micro-fuel cell. As observed in the existing literature [5,6], the zeta potential tends to change along the flow field as the fuel gets consumed in the chemical reaction occurring at the catalyst layer, adjoining the flow channels. The heterogeneous zeta potentials in microchannels can also be achieved through chemical modifications, coupled capillaries and integrated systems [8]. Hence, it is important to understand the flow behavior in the microchannel of the fuel cell under variable zeta potential conditions. To this end, the Poisson–Boltzmann and Navier–Stokes equations are solved numerically to investigate the electroosmotic driven flow phenomena for a range of operating conditions.

2. Physical problem

In Fig. 1 schematic of the serpentine microchannel model is shown. The channel considered here is a three dimensional serpentine channel. The cross sectional area of the channel is 100 μ m × 100 μ m. The model consists of a single 'S' shaped segment of the serpentine channel. It has three straight lengths connected by two semicircular arcs. In Fig. 1 length $L = 300\,\mu$m and the radius of curvature at bend is $R_c = 200\,\mu$m.

3. Governing equations

Electroosmosis is the motion of fluid caused by externally applied electric potential. In practice, most surfaces contain a

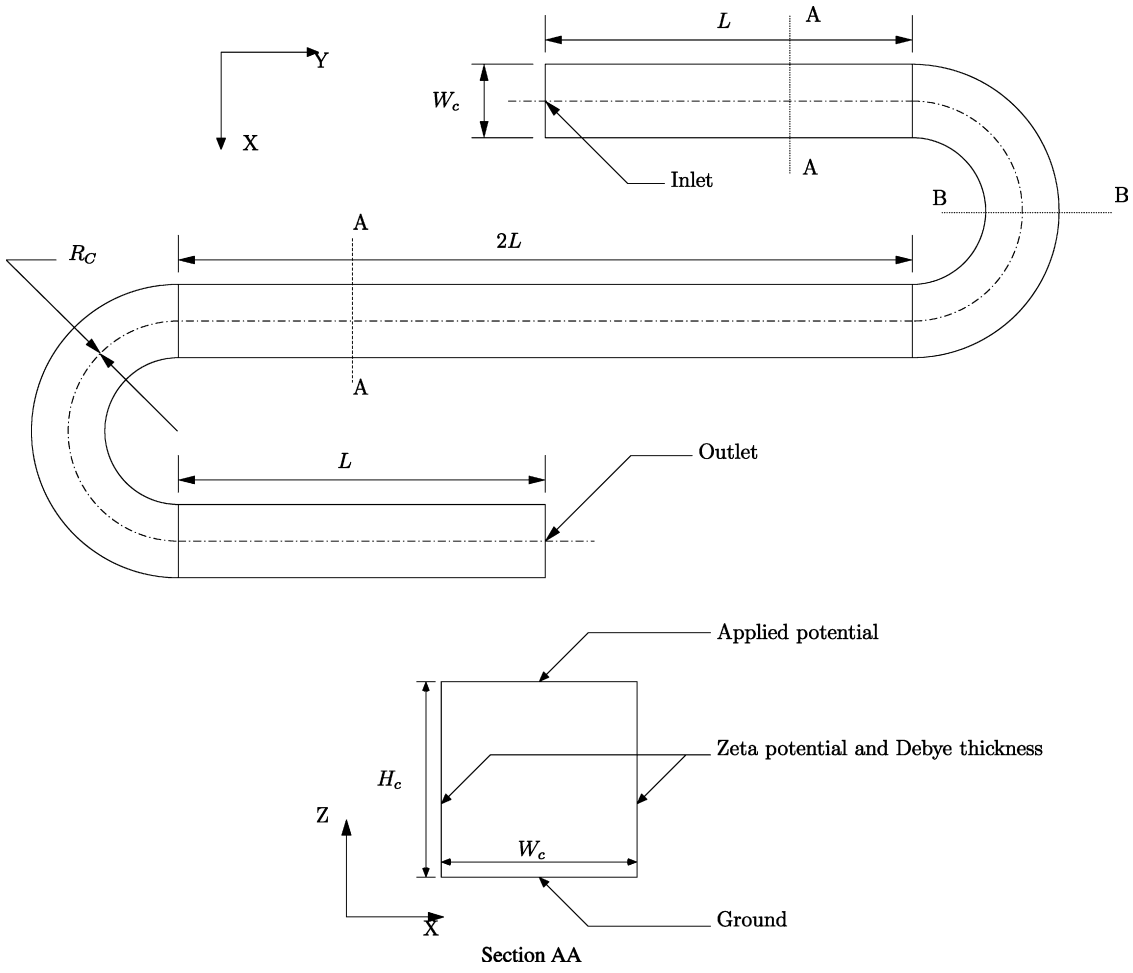

Fig. 1. Geometry of serpentine channel.

residual negative charge. When such charged surface comes in contact with ionizing fluid, the ions having polarity opposite to the surface charge are attracted towards the surface. These ions accumulate near the surface, forming an *electric double layer* (EDL). In this layer ion concentration changes from a maximum value (zeta potential, ζ_w) near the wall to a neutral state in the fluid core. The thickness of this layer is characterized by Debye length, λ, which is defined as the distance from the solid surface to which the charge drops to e^{-1} (37%) of its maximum value. The typical range of zeta potential and Debye length is 20–150 mV and 10^{-9} to 10^{-6} m, respectively [11,13]. When electric potential is applied across a capillary, the ions in the EDL move under the influence of the electric field. This ion movement causes bulk fluid motion due to the momentum transfer from EDL to the fluid core. Thus, the force acting on ions is accommodated as a body force in Navier–Stokes equation, which reads as

$$\rho(V \cdot \nabla)V = -\nabla P + \mu\nabla^2 V + \rho_E E \tag{1}$$

where ρ_E is the charge density and E is the electric field. For steady flow with constant properties, the continuity equation can be written as

$$\nabla \cdot V = 0 \tag{2}$$

The electric field E in Eq. (1) has two contributions. One is the field due to applied potential (ϕ) for which governing equation is

$$\nabla^2\phi = 0 \tag{3}$$

The second contribution is the field due to EDL which is governed by the equation

$$\nabla^2\psi = -\frac{\rho_E}{\epsilon} \tag{4}$$

The charge density is given by

$$\rho_E = FC_0 z_- e^{(z_- F\psi/R_u T)} - FC_0 z_+ e^{(z_+ F\psi/R_u T)} \tag{5}$$

which, for a symmetric electrolyte of valence number z_e becomes

$$\rho_E = 2FC_0 \sinh\left(\frac{z_e F\psi}{R_u T}\right) \tag{6}$$

where ψ is the potential due to electrical double layer, F the Faraday's constant, R_u is universal gas constant.

3.1. Boundary conditions

For fluid flow, a constant velocity corresponding to a given Reynolds number is specified at the channel inlet. At outlet, a

constant pressure (atmospheric) is specified. No slip boundary condition is imposed on all the remaining walls. Following is the mathematical representation of the above conditions:

$$\left.\begin{array}{l} u = 0 \\ v = \text{constant} \\ w = 0 \end{array}\right\}, \quad \text{for} \quad \begin{cases} 0 < x < 100\ \mu\text{m} \\ y = 0 \\ 0 < z < 100\ \mu\text{m} \end{cases}$$

$$P = 0, \quad \text{for} \quad \begin{cases} 4R_c\ \mu\text{m} < x < 4R_c + 100\,\mu\text{m} \\ y = 0\ \mu\text{m} \\ 0 < z < 100\ \mu\text{m} \end{cases}$$

$$\left.\begin{array}{l} u = 0 \\ v = 0 \\ w = 0 \end{array}\right\}, \quad \text{for all other boundaries}$$

For electric field, a fixed potential is specified at top and bottom walls of the channel, as shown in Fig. 1, which can be expressed as,

$$\phi = 0\,\text{V}, \quad \text{for} \quad \begin{cases} z = 0 \\ \text{for all } x \text{ and } y \end{cases}$$

$$\phi = 0.1\,\text{V}, \quad \text{for} \quad \begin{cases} z = 100\ \mu\text{m} \\ \text{for all } x \text{ and } y \end{cases}$$

A zeta potential and Debye length are specified on the side walls of the channel as shown in Fig. 1. The Debye length is kept constant at 1×10^{-7} m. The zeta potential is varied using stepwise, linear and constant profiles, to investigate the effect of zeta potential profile on the electroosmotic flow. Also, both walls are subjected to different zeta potential conditions. In total, seven different combinations are studied and it is expected that such variations in zeta potential are present in the actual operating micro-fuel cells. The variable zeta potential conditions can be expressed mathematically in the following manner:

Case 1: Constant zeta potential of −50 mV on both the side walls.

$\zeta_w = -50\,\text{mV}, \quad \text{for} \quad 0 < z < 100\ \mu\text{m}$ } On the left and right wall

Case 2: Stepwise zeta potential on right wall and constant zeta potential of −50 mV on the left wall.

$$\left.\begin{array}{ll} \zeta_w = -10\,\text{mV}, & \text{for} \quad 0 < z < 30\ \mu\text{m} \\ \zeta_w = -50\,\text{mV}, & \text{for} \quad 30\ \mu\text{m} < z < 70\ \mu\text{m} \\ \zeta_w = -90\,\text{mV}, & \text{for} \quad 70\ \mu\text{m} < z < 100\ \mu\text{m} \end{array}\right\} \text{On the right wall}$$

$\zeta_w = -50\,\text{mV}, \quad \text{for} \quad 0 < z < 100\ \mu\text{m}$ } On the left wall

Case 3: Stepwise zeta potential on left wall and constant zeta potential of −50 mV on the right wall.

$\zeta_w = -50\,\text{mV}, \quad \text{for} \quad 0 < z < 100\ \mu\text{m}$ } On the right wall

$$\left.\begin{array}{ll} \zeta_w = -10\,\text{mV}, & \text{for} \quad 0 < z < 30\ \mu\text{m} \\ \zeta_w = -50\,\text{mV}, & \text{for} \quad 30\ \mu\text{m} < z < 70\ \mu\text{m} \\ \zeta_w = -90\,\text{mV}, & \text{for} \quad 70\ \mu\text{m} < z < 100\ \mu\text{m} \end{array}\right\} \text{On the left wall}$$

Case 4: Stepwise zeta potential on left and right walls.

$$\left.\begin{array}{ll} \zeta_w = -10\,\text{mV}, & \text{for} \quad 0 < z < 30\ \mu\text{m} \\ \zeta_w = -50\,\text{mV}, & \text{for} \quad 30\ \mu\text{m} < z < 70\ \mu\text{m} \\ \zeta_w = -90\,\text{mV}, & \text{for} \quad 70\ \mu\text{m} < z < 100\ \mu\text{m} \end{array}\right\} \text{On the left and right walls}$$

Case 5: Linear zeta potential on right wall and constant zeta potential of −50 mV on the left wall.

$\zeta_w = -0.01 - \frac{0.09-0.01}{100\times10^{-6}} Z\,V, \quad \text{for} \quad 0 < z < 100\ \mu\text{m}$ } On the right wall

$\zeta_w = -50\,\text{mV}, \quad \text{for} \quad 0 < z < 100\ \mu\text{m}$ } On the left wall

Table 1
Boundary conditions for Cases 1–7

Case	Boundary conditions
Case 1	Constant zeta potential on both walls
Case 2	Stepwise zeta potential on right wall and constant zeta potential on left wall
Case 3	Stepwise zeta potential on left wall and constant zeta potential on right wall
Case 4	Stepwise zeta potential on both walls
Case 5	Linear zeta potential on right wall and constant zeta potential on left wall
Case 6	Linear zeta potential on left wall and constant zeta potential on right wall
Case 7	Linear zeta potential on both walls

Table 2
Properties of methanol

Physical property	Value	Dielectric property	Value
Density (kg m^{-3})	785	Electric conductivity (Ω m^{-1})	4.4×10^{-4}
Viscosity (Pa s)	5.6×10^{-4}	Relative permittivity	33.62

Case 6: Linear zeta potential on left wall and constant zeta potential of −50 mV on the right wall.

$$\left.\begin{aligned}\zeta_w &= -0.01 - \frac{0.09-0.01}{100\times10^{-6}} Z\,V, \quad \text{for} \quad 0 < z < 100\ \mu\text{m}\\ \zeta_w &= -50\,\text{mV}, \quad \text{for} \quad 0 < z < 100\ \mu\text{m}\end{aligned}\right\}$$

On the left wall / On the right wall

Case 7: Linear zeta potential on left and right walls.

$$\zeta_w = -0.01 - \frac{0.09-0.01}{100\times10^{-6}} Z\,V, \quad \text{for} \quad 0 < z < 100\ \mu\text{m}$$

On the left and right wall

These boundary conditions are also summarized in Table 1 for easy reference.

4. Numerical technique

The channel geometry is created and meshed using CFD-GEOM modeler. Structured grid is used for simulations. A grid independence study is carried out by successively refining the grid, increasing the number of elements in the domain. The grid is made extra fine in the near wall region where maximum gradients occur. For a grid having 260,431 elements, the solution is found to be grid independent. Hence this mesh size was used in all the cases. CFD software CFD-ACE+ is used for the simulations. Upwind scheme is used in the CGS + Pre solver [14] for velocity and electric field while AMG solver is used for pressure correction. Parametric solver is used to solve for values of inlet velocity corresponding to a range of Reynolds number. A Reynolds number of 0.001 is used in the simulations. Here, Reynolds number is defined as

$$Re = \frac{\rho V_{\text{inlet}} D_h}{\mu}$$

where D_h is the hydraulic diameter of the channel, defined as

$$D_h = \frac{4(W_c \times H_c)}{2(W_c + H_c)}$$

Here W_c is the width of the channel and H_c is the depth of the channel as shown in Fig. 1. The effect of zeta potential profile on the velocity profile in the channel is studied. The physical and dielectric properties of methanol at 25 °C used for simulations are provided in Table 2.

5. Results and discussion

The velocity vectors in the straight portion of the microchannel, at a distance of 150 μm from the channel inlet, is shown in Fig. 2. This represents the flow conditions under constant zeta potential applied at both walls (Case 1). The color indicates the velocity magnitude ($\sqrt{u^2 + v^2 + w^2}$) while the vectors in-

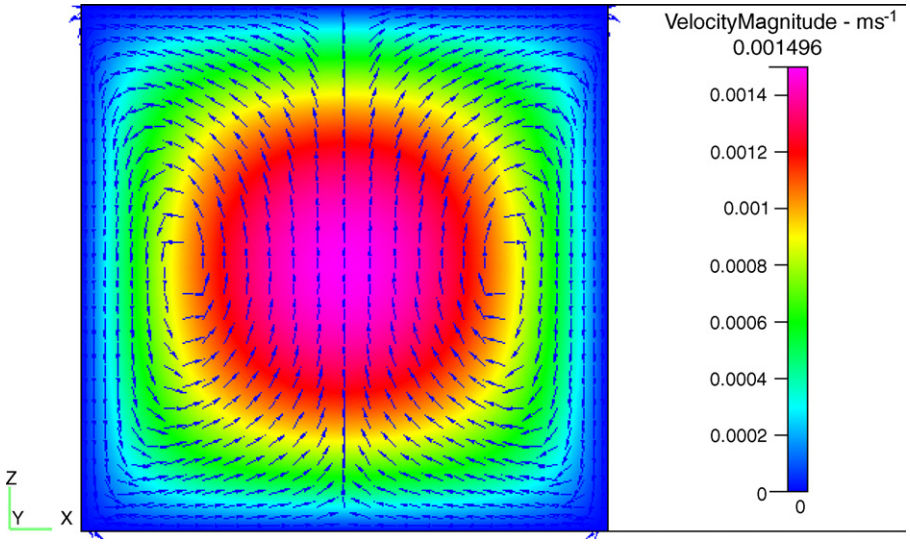

Fig. 2. Flow pattern in the channel cross section at 150 μm from channel inlet (section AA in Fig. 1) for Case 1.

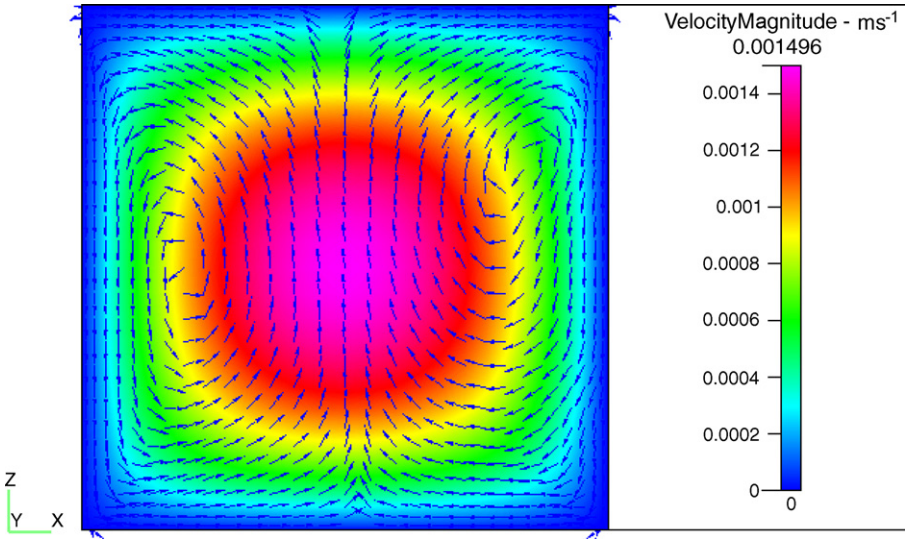

Fig. 3. Flow pattern in the channel cross section at 150 μm from channel inlet (section AA in Fig. 1) for Case 2.

dicate direction of in-plane component ($\sqrt{u^2 + w^2}$). It can be seen that due to electroosmotic driving force, a secondary vortex pair has been generated in the flow cross section such that the fluid near the side walls moves towards the bottom plate. The fluid again rises in the central portion of the channel to maintain the continuity. Thus two distinct vortices are formed due to electroosmosis. These kind of vortices are absent in case of flow without electroosmosis. This modified flow profile gives rise to additional pressure drop in case of flow with electroosmosis [12].

Figs. 3 and 4 show the velocity patterns for Cases 2 and 3, respectively. It is observed that due to the stepwise zeta potential profile applied on the right wall, the center of the right vortex is shifted upwards in Fig. 3 compared to Fig. 2. This is because for Case 2, the maximum magnitude of zeta potential occurs in the top region (−90 mV) while in the bottom region it is minimum (−10 mV). Hence, the top region dominates the electroosmosis-induced secondary flow and the vortex center is shifted towards the top. Similar behavior is observed in Case 3 where stepwise zeta potential is applied on the left wall.

It is interesting to observe the flow pattern for Case 4, which is shown in Fig. 5, where stepwise zeta potential is applied on both the side walls. Under such condition, the centers of both the secondary vortices are shifted towards the top wall.

When the zeta potential is linearly varied for each wall, as shown in Figs. 6 and 7, there is a gradual change in the electroosmotic driven force on the fluid. This results in shifting of

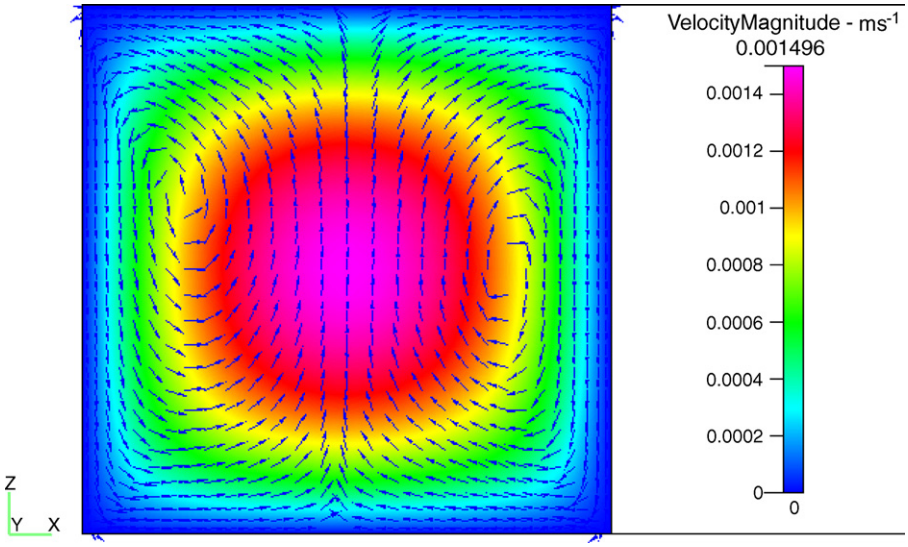

Fig. 4. Flow pattern in the channel cross section at 150 μm from channel inlet (section AA in Fig. 1) for Case 3.

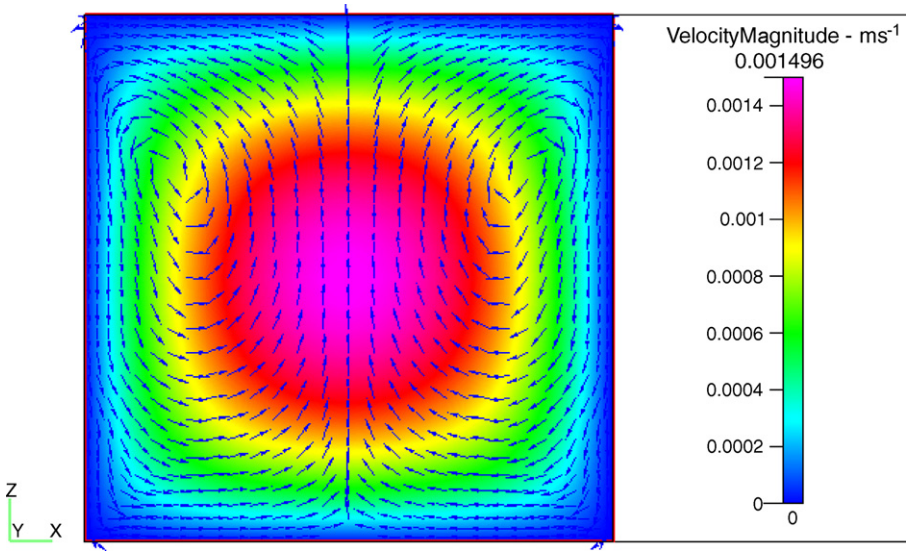

Fig. 5. Flow pattern in the channel cross section at 150 μm from channel inlet (section AA in Fig. 1) for Case 4.

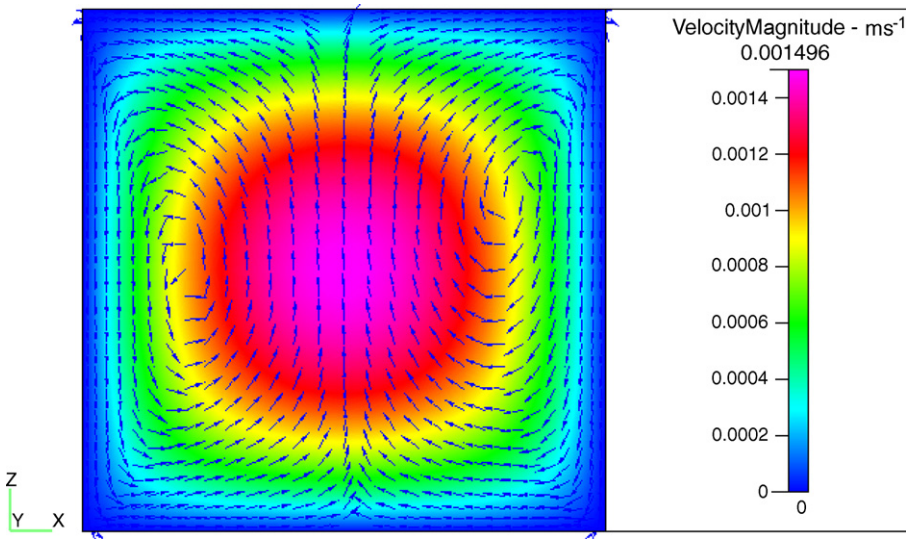

Fig. 6. Flow pattern in the channel cross section at 150 μm from channel inlet (section AA in Fig. 1) for Case 5.

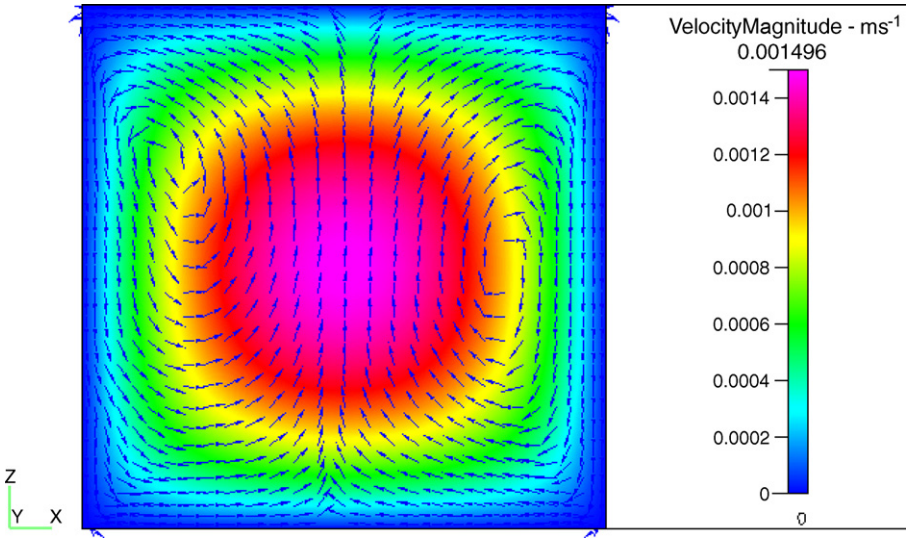

Fig. 7. Flow pattern in the channel cross section at 150 μm from channel inlet (section AA in Fig. 1) for Case 6.

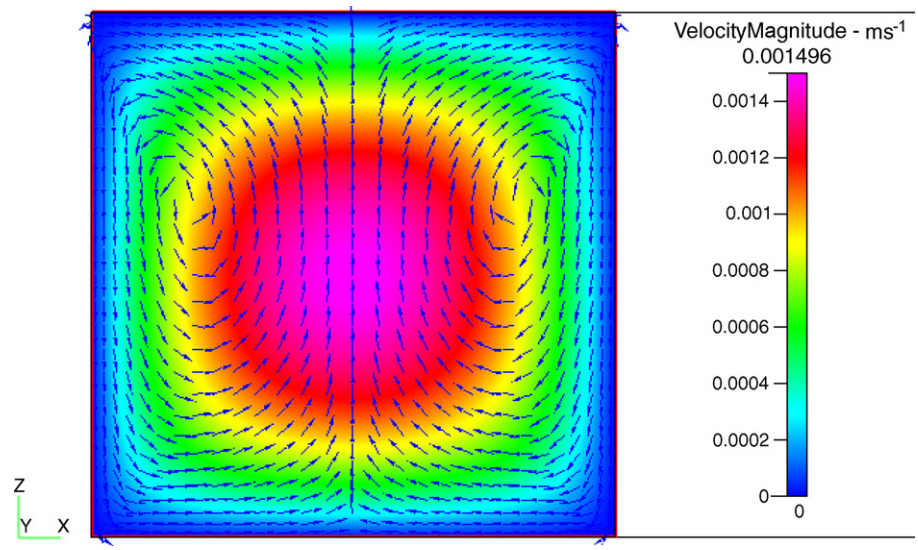

Fig. 8. Flow pattern in the channel cross section at 150 μm from channel inlet (section AA in Fig. 1) for Case 7.

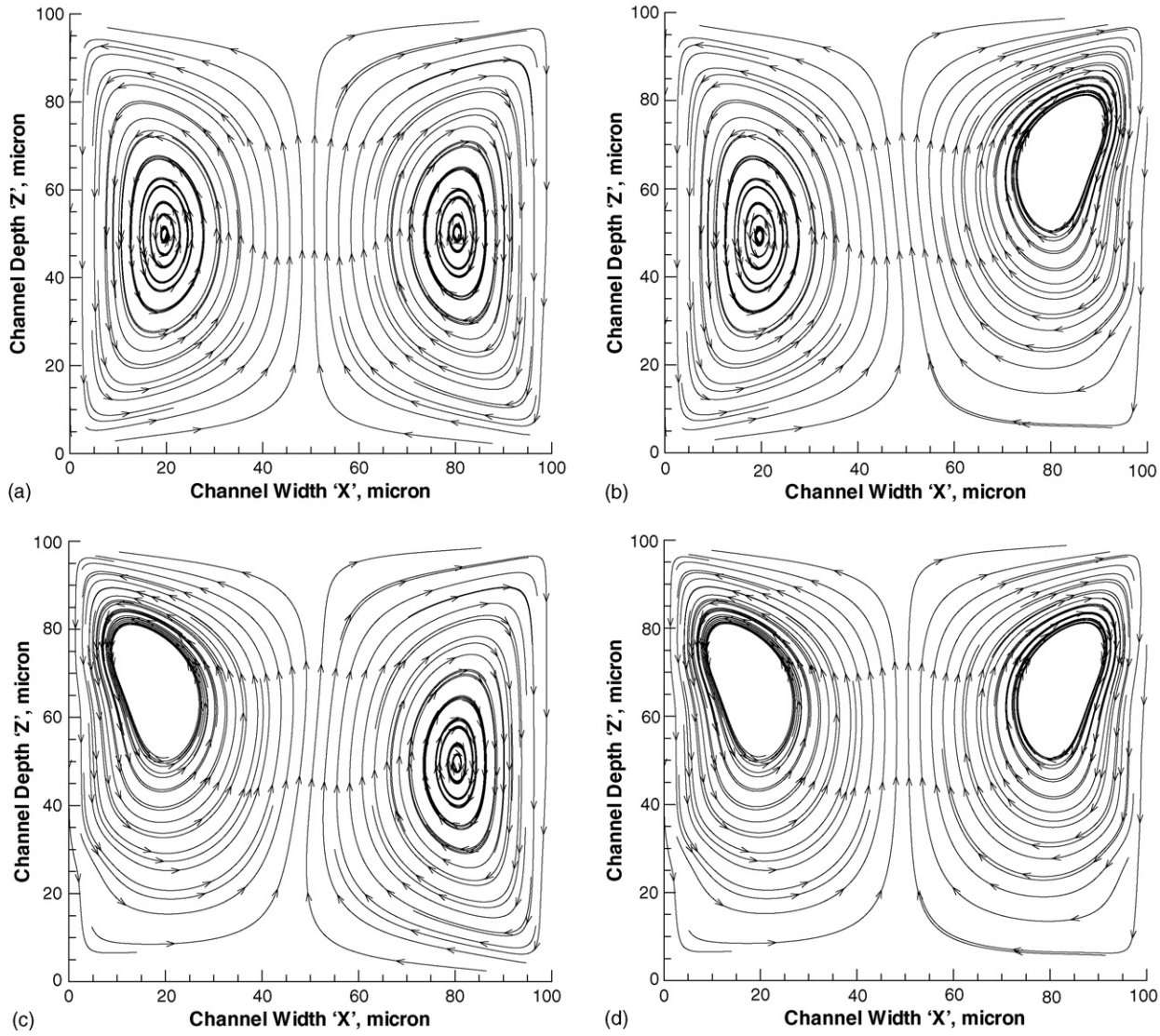

Fig. 9. Streamline plots in the channel cross section at 150 μm from channel inlet (section AA in Fig. 1) for Cases 1–7: (a) Case 1; (b) Case 2; (c) Case 3; (d) Case 4; (e) Case 5; (f) Case 6; (g) Case 7.

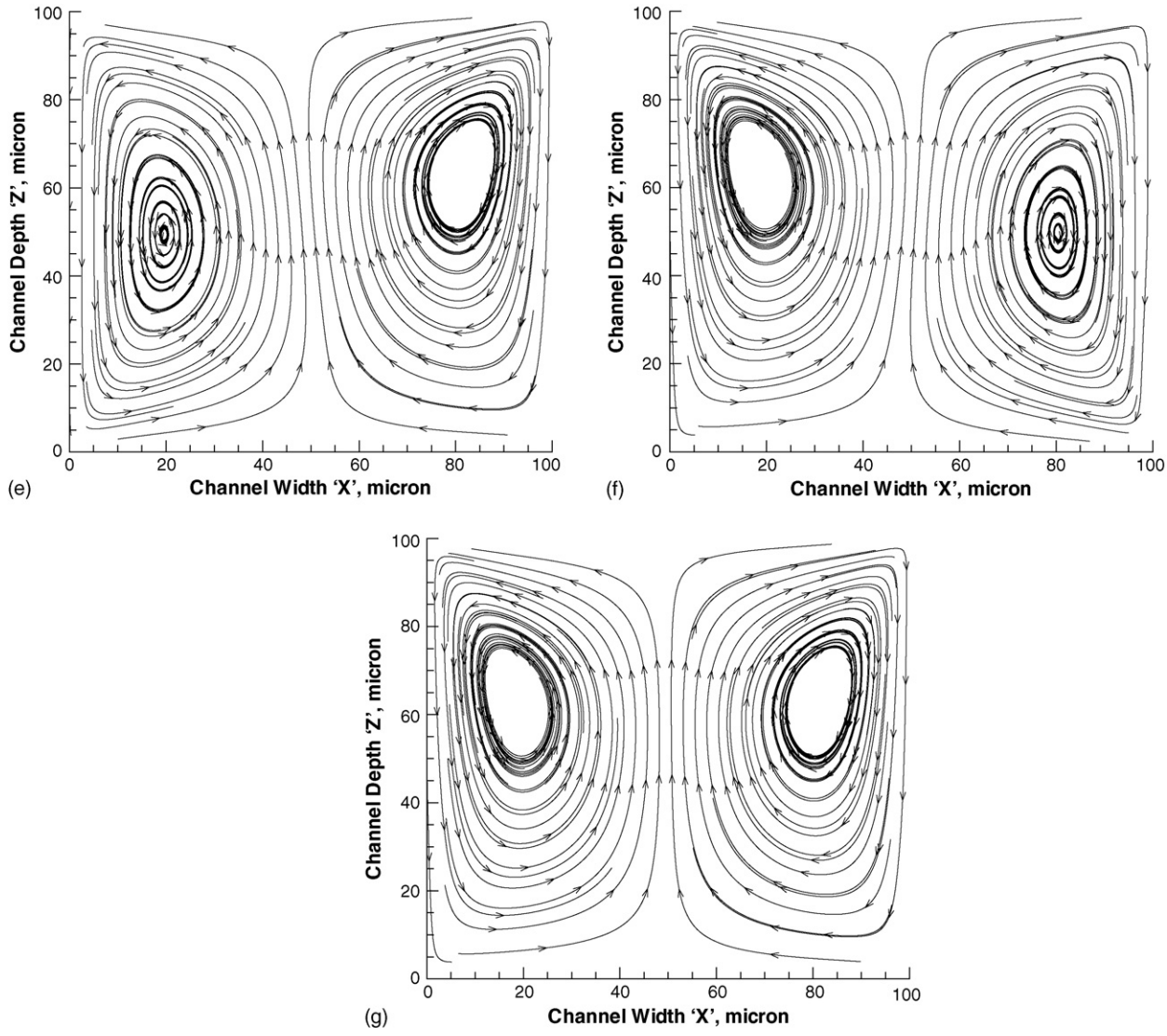

Fig. 9. (*Continued*).

the secondary vortex by a smaller distance as compared to Cases 2–4. Fig. 7 shows the velocity profile for Case 6, in which zeta potential is linearly varied along the left wall and in Fig. 8, the zeta potential is linearly varied along both the side walls.

The streamline plots for all Cases 1–7 are shown in Fig. 9(a–g). The streamline plots depict the formation of vortices for all the cases, and the effect of variable zeta potential is clearly seen in these figures.

Fig. 10 shows the variation of x component of velocity along the channel width at $z = 50\ \mu m$ for the cross section AA under various zeta potential conditions. It is observed here that for Case 1, the u component is zero as the secondary vortices appear at the center line and results in a zero velocity at the central core. For Cases 2 and 3, the u component reaches maximum near the vortex core and then it drops to zero towards the outer edge of the vortex. It is to be noted that due to the shifting of the vortex core, the location of the maxima is at two different positions along the channel width. However, when both walls are subjected to the stepwise variable zeta potential, as in Case 4, the u component has two maxima near each vortex core, and the profile is bounded between the velocity profiles for Case 2 and 3, respectively. Similar behavior is observed for Cases 5 and 6, where linear variation of zeta potential is applied at the each wall and for Case 7, where both walls are subjected to a variable zeta potential. It is to be noted that linear variation of zeta potential results in lower electroosmotic velocity, which is observed in Fig. 10, where the magnitude of u component is lower for Cases 5–7 compared to Cases 2–4.

The y component of velocity is plotted in Fig. 11 along the channel width at $z = 50\ \mu m$ for the cross section AA. It is observed that the velocity profile corresponds to a fully developed profile of steady laminar flows in square ducts for all the cases. The y component is predominantly due to the pressure driven flow through the microchannel and the electroosmosis contribution to this velocity component is quite small and not discernible in the figure.

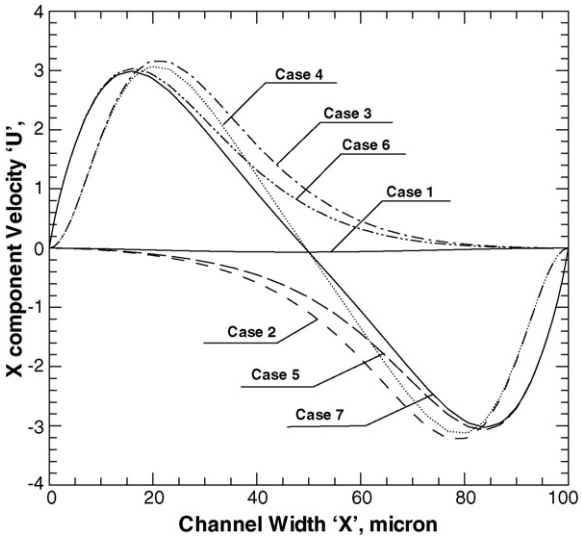

Fig. 10. Variation of x component of velocity at $z = 50\,\mu m$ along the channel width at section AA.

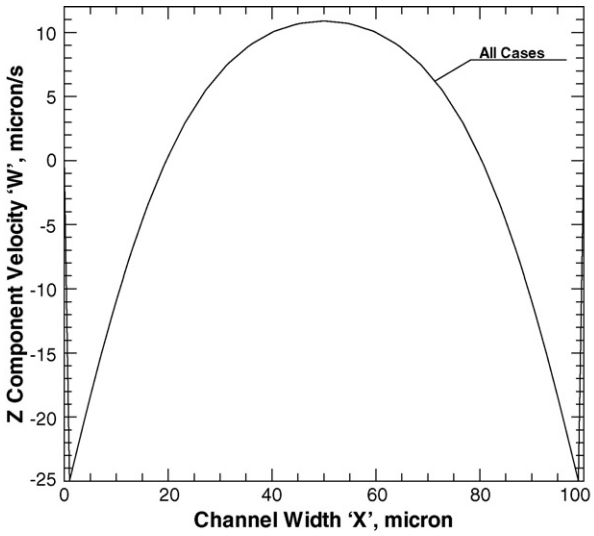

Fig. 12. Variation of z component of velocity at $z = 50\,\mu m$ along the channel width at section AA.

Fig. 12 shows the z component of velocity along the channel width at $z = 50\,\mu m$. It is observed that the z component reaches a maximum at a small distance from the wall where the electroosmotic velocity is maximum. It then drops to zero and again reaches a maximum value in opposite direction at the center of the channel. The variation of z component is similar for all the cases. This is in parallel with the velocity vector observed earlier, where the flow reverses and reaches its maximum value at the center of the channel.

The flow behavior at the semi-circular bend for section BB in Fig. 1 has also been studied for four different cases. Fig. 13(a–d) shows the streamline plots at the bend for pressure driven flow and the applied zeta potential of -0.1, -1 and $-50\,mV$ (i.e., Case 1), respectively. Fig. 13(a) shows the formation of vortices purely due to the pressure-driven flow with no contribution from the electroosmotic effect. As the applied zeta potential is increased at the semi-circular bend (section BB in Fig. 1), the electroosmotic forces cause the vortices to shift in a clockwise direction as shown in Fig. 13(d). The observed shift of secondary vortices in a clockwise direction with an increase in the applied zeta potential presents an excellent opportunity for obtaining flow control in the serpentine microchannel by regulating the zeta potential at the bend. Formation of additional vortices at the top left and bottom right corners has also been observed when the applied zeta potential is $-0.1\,mV$, as shown in Fig. 13(b).

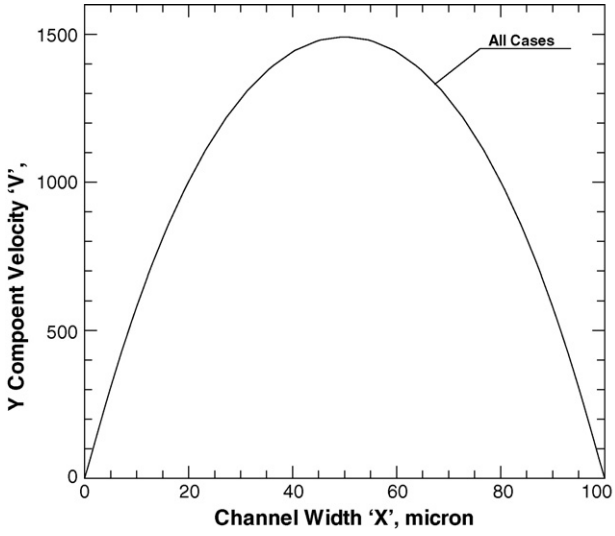

Fig. 11. Variation of y component of velocity at $z = 50\,\mu m$ along the channel width at section AA.

Fig. 14 shows the z component of velocity along the channel width at $z = 50\,\mu m$ for the cross section BB. It is observed here that for a pressure-driven flow only, the z component velocity is zero as the secondary vortices appear at the center line and results in a zero velocity at the central core. It is found that the z component reaches a maximum at a small distance from the wall when zeta potential of -0.1, -1 and $-50\,mV$ is applied on the side walls. The maximum velocity is reached for the $-50\,mV$ of applied zeta potential and decreases in magnitude as the applied zeta potential is reduced. The velocity component then drops to zero and again reaches a maximum value in opposite direction at the center of the channel. Hence, it can be concluded that the z component velocity influences the formation of vortices in the semi-circular bend at the cross section BB and results in the shifting of the vortices in the clockwise direction.

It is to be noted that the x and y components of velocity profile correspond to a fully developed velocity profile of steady laminar flows in square ducts for all the cases in the semi-circular bend. The velocity components are predominantly due to the pressure-driven flow through the microchannel and the electroosmotic contribution is quite negligible. However, an offset is observed in the peak velocity from the central axis towards the inner wall, which is due to the centrifugal forces dominating at the cross section of the bend.

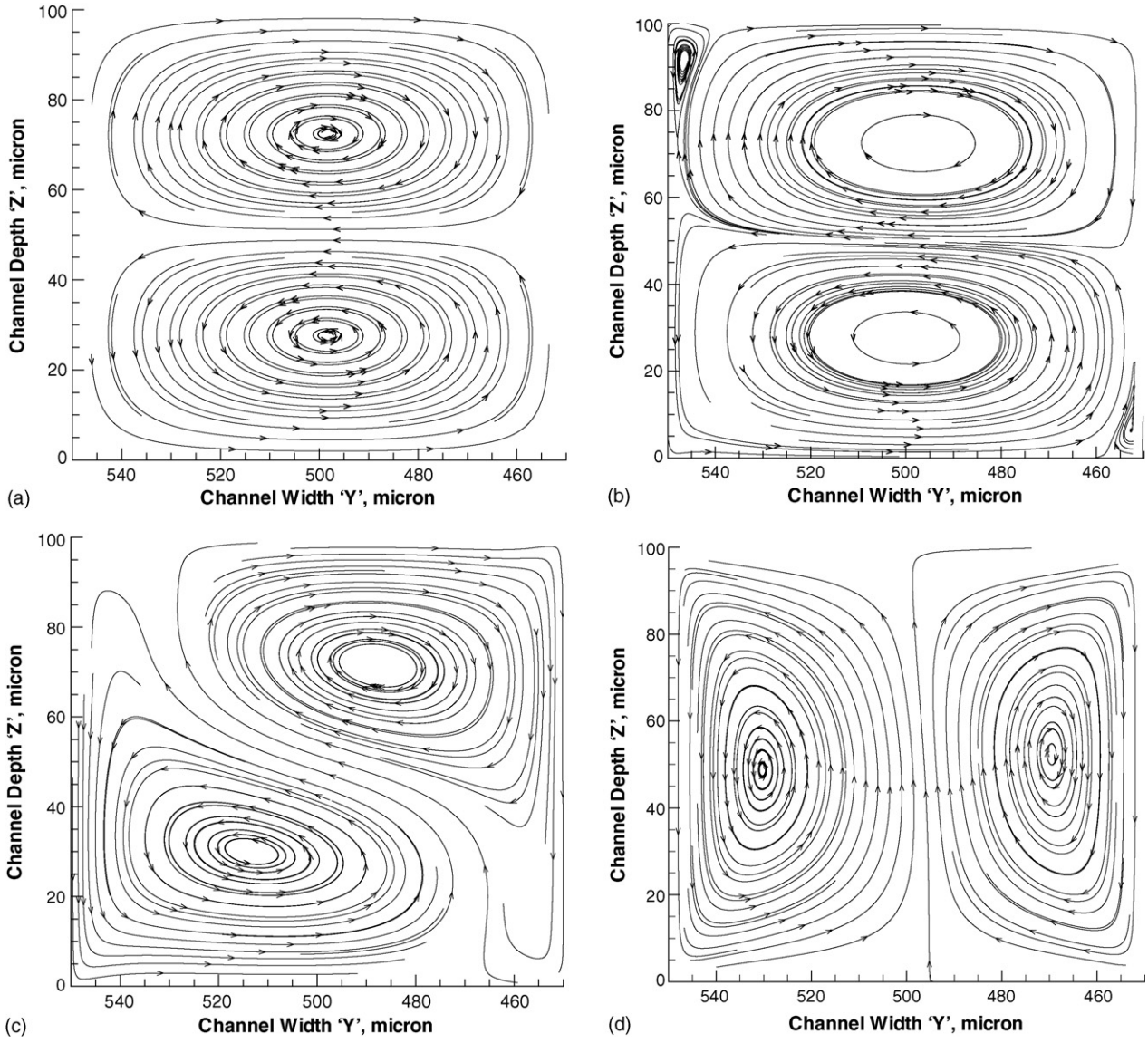

Fig. 13. Streamline plots in the channel cross section at the bend (section BB in Fig. 1) for different zeta potential values: (a) pressure driven flow; (b) 0.1 mV; (c) 1 mV; (d) 50 mV.

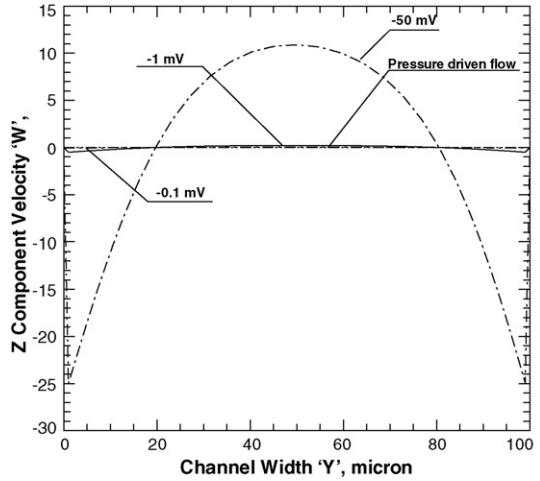

Fig. 14. Variation of z component of velocity at $z = 50\,\mu$m along the channel width at section BB.

6. Conclusions

A three-dimensional numerical simulation of flows through serpentine microchannels has been carried out for the channel side walls subjected to variable zeta potentials. Different boundary conditions with respect to the zeta potential – viz., stepwise and linear profiles, are applied at the side walls. It is observed that vortices are developed at the straight portion of the microchannel due to the electroosmosis and the characteristics of the vortices are quite different as compared to a constant zeta potential condition. The core of the vortices shifts when variable zeta potentials are applied at both the side walls of the channel. It is also observed that the magnitude of the electroosmosis-driven flow becomes smaller for the linear variation of zeta potential. Flow control in the serpentine microchannel by regulating the zeta potential at the bend has also been demonstrated. Formation of additional vortices at the top left and bottom right corners of the serpentine microchannel has been observed

at the semi-circular bend for very low values of applied zeta potential.

Acknowledgment

The support of Suman Mashruwala μ Engineering Laboratory, IIT Bombay is highly appreciated. The author, S.K. Mitra, acknowledges the Visiting Professorship at University of Waterloo, during which a part of this work was carried out.

References

[1] A.S. Rawool, S.K. Mitra, S.G. Kandlikar, Microfluidics Nanofluidics 2 (2006) 215–221.
[2] R. Probstein, Physicochemical Hydrodynamics, Wiley, New York, 1994.
[3] G. Karimi, X. Li, J. Power Sources 140 (2005) 1–11.
[4] L.M. Fu, J.Y. Lin, R.J. Yang, J. Colloid Interface Sci. 258 (2003) 266–275.
[5] A.E. Herr, J.I. Molho, J.G. Santiago, M.G. Mungal, T.W. Kenny, Anal. Chem. 72 (2000) 1053–1057.
[6] X. Chen, Y.C. Lam, X.Y. Chen, J.C. Chai, C. Yang, Numerical Simulation of Electroosmotic Flow with Step Change in Zeta Potential, https://dspace.mit.edu/bitstream/1721.1/7457/1/IMST018.pdf, accessed on 21 August 2006.
[7] J.S.H. Lee, C.L. Ren, D. Li, Anal. Chim. Acta 530 (2005) 273–282.
[8] J. Zhang, G. He, F. Liu, Phys. Rev. E 73 (2006) 050301.
[9] D. Souders, I. Khan, G.F. Yao, A. Incognito, M. Corrado, Seventh International Symposium on Fluid Control, Measurement and Visualization, 2003, pp. 1–7.
[10] C.R. Buie, Y. Banin, T. Chuyang, J.G. Santiago, F.B. Prinz, B.L. Pruitt, 19th IEEE International Conference on Micro Electro Mechanical Systems, 2006, pp. 938–941.
[11] J.A. Brant, K.M. Johnson, A.E. Childress, J. Membr. Sci. 2 (2005) 286–294.
[12] A.S. Rawool, S.K. Mitra, Microfluidics Nanofluidics 2 (2006) 261–269.
[13] B. Liechty, B.W. Webb, R.D. Maynes, Int. J. Heat Mass Transfer 48 (2005) 2360–2371.
[14] CFD-ACE+ Software Manuals, CFD Research Corporation, 2002.